Impact Failure Analysis of Reinforced Concrete Structural Components by Using Finite Element Method

A. Ramachandra Murthy[1], G.S. Palani[1], Nagesh R. Iyer[1], Smitha Gopinath[1] and V. Ramesh Kumar[1]

Abstract: This paper presents the details of projectile impact on reinforced concrete structural components. Nonlinear explicit transient dynamic analysis has been carried out by using finite element method. Concrete damage model has been employed to represent the nonlinear behaviour of target under impact load. Various methods of modeling of reinforcement have been explained. A brief note on equation of state for concrete, contact algorithms and nonlinear explicit transient dynamic analysis has been given. Numerical studies have been carried out to compute the response of concrete target due to impact of projectile. The computed penetration depth have been compared with the corresponding experimental observations and found that they are in good agreement with each other. Further, parametric studies have been conducted for various grades of concrete, caliber radius head and design expressions have been proposed to compute the penetration depth.

Keywords: Impact analysis, Concrete damage model, Contact algorithm, Nonlinear transient dynamic analysis, Finite element analysis

1   Introduction

Concrete is a widely used material in civil and defense constructions. Potential missiles/projectiles include kinetic munitions, vehicle and aircraft crashes, fragments generated by military and terrorist bombing, fragments generated by accidental explosions and other events (e.g. failure of a pressurized vessel, failure of a turbine blade or other high-speed rotating machines), flying objects due to natural forces (tornados, volcanoes, meteoroids), etc. These projectiles vary broadly in their shapes and sizes, impact velocities, hardness, rigidities, impact attitude (i.e. obliquity, yaw, tumbling, etc.) and produce a wide spectrum of damage in the target. The interest in penetration, perforation and fragmentation of plain and

---

[1] CSIR-Structural Engineering Research Centre, CSIR Campus, Taramani, Chennai-113. E-mail: {murthyarc, pal, nriyer, smithag, ramesh} @serc.res.in

reinforced concrete (RC) targets arises from their use as barriers to protect civilian buildings and as bunkers to protect against impacts. Good barrier design practice consists of (i) preventing excessive local damage, and (ii) preventing collapse of the barrier resulting from its inability to withstand the absorbed energy. To prevent excessive local damage either the wall be thick enough to prevent scabbing of the concrete or that a properly designed 'scab' plate be attached to the rear surface of the wall. If a 'scab' plate is used, the wall should be sufficiently thick to prevent perforation. Overall wall collapse is prevented by designing the wall to have reserve strain energy capacity greater than the total absorbed energy to which it is subjected.

Numerous studies were carried out in the last 15 years for the development and improvement of the macro-scale concrete models for high-pressure applications [Govindjee et al. 1995; Malvar et al. 1997; Govindjee 1994; Malvar et al. 1996, 1994; Hentz et al. 2004; , Yonten et al. 2005]. Various material models were proposed, from relatively simple to more sophisticated ones and their capabilities in describing the actual nonlinear behaviour of the material under different loading conditions vary. Besides, because of the general complexity of the models, the determination of the model parameters (i.e., the model parameterization) also plays an important role in the actual performance of these models. This requires a sufficient understanding of the material formulation and the associated considerations. There are three important methods for studying local effects [Farnam et al. 2010; Rama chandra murthy et al. 2008, 2009] on a concrete target arising from projectile impact, namely experimental, analytical and numerical methods. Experimental data are always of importance extending the understanding of impact phenomena and for validating analytical and numerical models. Empirical formulae based on experimental data are especially important due to the simplified expressions to represent complexity of the phenomena. Several design codes employ empirical formulae for the design of protective barriers. Simple and accurate analytical models can be developed, when the underpinning mechanics of the local effects of the missile impact are understood. This approach offers the most efficient and economic way of predicting impact effects and helps to extend the range of validity of experimentally based empirical formulae. With the rapid developments of computational tools, computational mechanics and material constitutive models, the numerical simulation of local projectile impact effects becomes more reliable and economic. A number of commercial hydro codes such as AUTODYN (2001) and LS-DYNA (2003) are available for the general simulation of nonlinear dynamic responses. However, such simulations can produce reliable results for concrete structures, only if a material model capable of representing the essential mechanical processes of the material under varying stress and loading rate condi-

tions is available. It is observed from the literature that the concrete damage model is widely used for impact analysis of concrete structural components. But the impact studies carried out on RC structural components by using concrete damage model are less.

The objective of this paper is to present the details of the concrete damage model and to conduct nonlinear transient dynamic analysis for plain and RC structural components. Further, parametric studies have been carried out to compute the penetration depth by varying grade of concrete, caliber radius head and impact velocities towards proposing design expressions to compute penetration depth.

2 Concrete damage material model for impact analysis

The material models for concrete-like materials generally share in common some basic features of brittle materials such as pressure hardening, strain hardening and strain rate dependency. However, for simplicity, some models adopt highly restrictive assumptions; consequently, their applicability is limited to a certain class of problems. In cases, where the loading environment of the material is very complex and cannot be pre-defined, more robust material models that are capable of describing the varying concrete material behavior under different loading conditions are desired. It is observed from the literature [Farnam et al. 2010] that concrete damaged model is widely employed for simulation of non-linear behaviour of concrete. The details of the model are given below.

2.1 Concrete Damage Model

The concrete damage model was first developed for DYNA3D [Malvar et al. 1997; Govindjee 1994; Malvar et al. 1996] software. The concrete damage model uses three independent strength surfaces, namely, an initial yield surface, a maximum failure surface and a residual surface, with consideration of all the three stress invariants (I_1, J_2 and J_3). The strength surfaces are uniformly expressed as:

$$\Delta\sigma = \sqrt{3J_2} = f(p, J_2, J_3) \tag{1}$$

where $\Delta\sigma$ and p denote, respectively, the principal stress difference and pressure, and

$$f(p, J_2, J_3) = \Delta\sigma^c * r' \tag{2}$$

where $\Delta\sigma^c$ represents the compressive meridian and r' can be calculated by using the formula given below.

$$r' = \frac{r}{r_c} = \frac{2(1-\psi^2)\cos\theta + (2\psi-1)\sqrt{4(1-\psi^2)\cos^2\theta + 5\psi^2 - 4\psi}}{4(1-\psi^2)\cos^2\theta + (1-2\psi)^2} \tag{3}$$

where $\psi = r_t/r_c$ (refer to Figure 1). The Lode angle θ is a function of the second and third deviatoric stress invariant and can be obtained by either of the following two equations:

$$\cos\theta = \frac{\sqrt{3}}{2}\frac{s_1}{\sqrt{J_2}} \text{ or } \cos 3\theta = \frac{3\sqrt{3}}{2}\frac{J_3}{J_2^{3/2}} \tag{4}$$
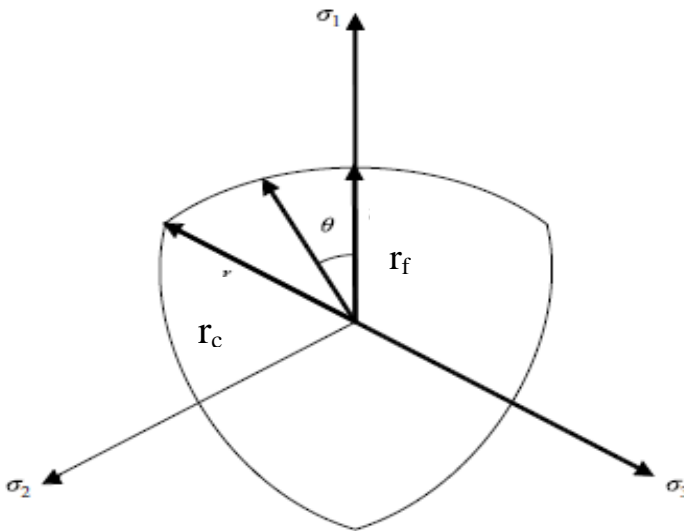

Figure 1: Typical deviatoric cross-section of strength surface

The compressive meridians of the initial yield surface $\Delta\sigma_y^c$, the maximum failure surface $\Delta\sigma_m^c$ and the residual surface $\Delta\sigma_r^c$ are defined independently as:

$$\Delta\sigma_y^c = a_{0y} + \frac{p}{a_{1y} + a_{2y}p} \tag{5}$$

$$\Delta\sigma_m^c = a_0 + \frac{p}{a_1 + a_2 p} \tag{6}$$

$$\Delta\sigma_r^c = \frac{p}{a_{1f} + a_{2f}p} \tag{7}$$

The eight free parameters, namely, a_{0y}, a_{1y}, a_{2y}, a_0, a_1, a_2, a_{1f}, and a_{2f} are to be determined from experimental data. With the specification of the three strength

surfaces, the loading surfaces representing strain hardening after yield are defined as:

$$\Delta\sigma_L = \eta\Delta\sigma_m + (1 - \eta)\Delta\sigma_y \tag{8}$$

The post-failure surfaces, denoted by $\Delta\sigma_{pf}$, are defined in a similar way by interpolating between the maximum failure surface $\Delta\sigma_m$ and the residual surface $\Delta\sigma_1$:

$$\Delta\sigma_{pf} = \eta\Delta\sigma_m + (1 - \eta)\Delta\sigma_r \tag{9}$$

The variable η in eqns. (8) and (9) is called the yield scale factor, which is determined by a damage function λ:

$$\lambda = \begin{cases} \int_0^{\bar{\varepsilon}_p} \frac{d\bar{\varepsilon}_p}{[1+p/f_t]^{b1}} & p \geq 0 \\ \int_0^{\bar{\varepsilon}_p} \frac{d\bar{\varepsilon}_p}{[1+p/f_t]^{b2}} & p < 0 \end{cases} \tag{10}$$

where f_t is the quasi-static concrete tensile strength, $d\bar{\varepsilon}_p$ is effective plastic strain increment, and $d\bar{\varepsilon}_p = \sqrt{\frac{2}{3}d\varepsilon_{ij}^p d\varepsilon_{ij}^p}$ with $d\varepsilon_{ij}^p$ being the plastic strain increment tensor.

It is to be noted that the damage function has different definitions for compression ($p \geq 0$) and tension ($p < 0$) to account for different damage evolution of concrete in tension and compression. The evolution of the yield scale factor η follows a general trend: it varies from "0" to "1", when the stress state advances from the initial yield surface to the maximum failure surface, and changes from "1" back to "0", when the stress softens from the failure surface to the residual surface.

2.2 Equation of state (EOS) for concrete

For the hydrocode analysis, an equation of state is required as a separate entity in the material description, in addition to the constitutive model discussed in the preceding sections. EOS plays the role of linking together three inter-independent thermodynamic quantities, namely, pressure p, density ρ and internal energy e.

To obtain a proper EOS for concrete is a challenging task as concrete exhibits a very complex volumetric response due to its inherent non-homogeneity and the porosity of the material. When concrete is subjected to quasi-static or low dynamic loads, the internal energy term can be neglected from the EOS due to its insignificance when pressure is low. While this EOS proves to be capable of representing the concrete thermodynamic behaviour at high pressures, it also allows for a reasonably detailed description of the compaction behaviour at low pressure ranges. It

is established on the premise that the initial specific internal energy for the porous material is the same as the solid material under the same pressure and temperature.

The equation of state of the fully compacted or solid material is described with a polynomial function as:

$$p(\rho, E) = A_1 \mu + A_2 \mu^2 + A_3 \mu^3 + (B_0 + B_1 \mu) \rho_0 e \tag{11}$$

where $\mu = (\rho/\rho_0 - 1)$ is the relative volume change; a_1, a_2, a_3, B_0 and B_1 are constants to be determined; ρ_0 is the reference initial density of the solid material and e denotes the specific internal energy. The EOS for the porous material is then calculated by substituting a new variable $\rho_p x \alpha$ for ρ in eqn. (11), i.e.,

$$p(\rho_p, E, \alpha) = A_1 \overline{\mu} + A_2 \overline{\mu}^2 + A_3 \overline{\mu}^3 + (B_0 + B_1 \overline{\mu}) \rho_0 e \tag{12}$$

where ρ_p is the density of the porous material, $\overline{\mu} = \rho_p \alpha / \rho_0 - 1$, and α is called material "porosity" and is defined as $\alpha = v_p/v_s$ in which v_p and v_s refer, respectively, to the specific volume of the porous and solid material at the same pressure and temperature. Physically, α is a function of the material thermodynamic state and can be expressed in a general form as:

$$\alpha = g(p, e) \tag{13}$$

There is a general lack of sufficient test data to evaluate eqn. (13) and the shock Hugoniot can be used to provide a relation between p and e. Thus, α becomes only a function of p. In $P - \alpha$ EOS, $\alpha(p)$ is defined as:

$$\alpha = 1 + (\alpha_{ini} - 1) \left[(p_{lock} - p) / (p_{lock} - p_{crush}) \right]^n \tag{14}$$

In the above expression, α_{ini} is the initial porosity of the intact concrete; p_{crush} corresponds to the pore collapse pressure beyond which concrete plastic compaction occurs and p_{lock} is the pressure at which the concrete porosity α reaches unity. In the numerical calculation, an iterative procedure has to be implemented in order to solve for the current pressure value as the pressure p is involved implicitly in eqn. (12).

It is worth pointing out that the construction of an equation of state such as $p - \alpha$ EOS described above is independent of the material constitutive models and, therefore, it can be used with any material model.

3 Contact algorithms

Several contact algorithms are available in the literature, namely, frictional sliding, single surface contact, nodes impacting on a surface, tied interfaces, one-dimensional slide lines, rigid walls, material failure along interfaces, penalty and

Lagrangian projection options for constraint enforcement and fully automatic contact. Details of, 'contact-automatic-single-surface' algorithm are presented below.

This algorithm uses a penalty method to model the contact interface between the different parts. In this approach, the slave and master surfaces are generated automatically within the code. The method consists of placing normal interface springs to resist interpenetration between element surfaces. An example of this approach is illustrated in Figure 2. As shown in Figure 2, when a slave node penetrates a master surface in a time step, the code automatically detects it, and applies an internal force to the node (indicated by the spring) to resist penetration and keep the node outside the surface. The internal forces added to the slave nodes are a function of the penetrated distance and a calculated stiffness for the master surface. The stiffness is computed as a function of the bulk modulus, volume and face area of the elements in the master surface. A static and dynamic coefficient of friction of 0.8 is used generally between the different parts in contact.

$$F_s = k_s x_p$$

$$k_s = \alpha \, K_B \frac{A_e^2}{V_e}$$
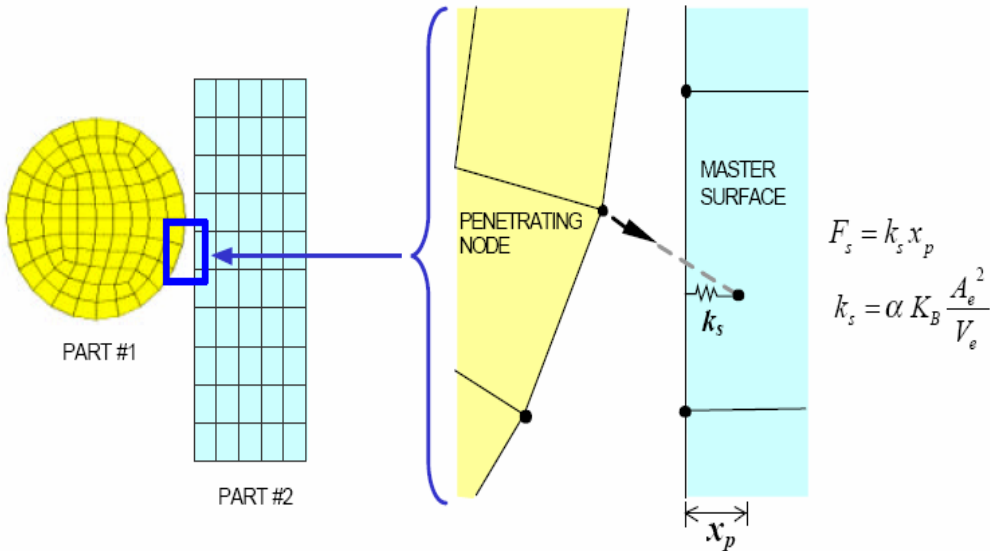
Figure 2: Penalty method for contact algorithm

4 Modelling of reinforcement

Finite element models for reinforced concrete structures have generally been based on replacing the composite continuum by an assembly of elements representing the concrete and the steel reinforcement. Presently, three alternative techniques are mainly used for modeling reinforcement in a three-dimensional finite element model of a concrete structure: the discrete model, the embedded model and the smeared model. The desired technique is chosen depending on the application and the degree of detail to which the effect of reinforcement needs to be considered. However, most of the difficulties in modeling reinforced concrete behavior rely in the development of an effective and realistic concrete material formulation and not in the modeling of the reinforcement.

4.1 Discrete Model

In the discrete model, reinforcement is modeled by using bar or beam elements connected to the concrete mesh nodes. As a result, there are "shared nodes" between the concrete mesh and the reinforcement mesh, as shown in Figure 3. Also, since the reinforcement is superimposed in the concrete mesh, concrete exists in the same regions occupied by the reinforcement. The drawback of using the discrete model is that the concrete mesh is restricted by the location of the reinforcement. Full bond is generally assumed between the reinforcement and the concrete. In cases where bond issues are of importance, fictitious spring elements are used to model bond-slip between the concrete and the reinforcement elements. These linkage elements connect concrete nodes with reinforcement nodes having the same coordinates. These type of elements have no physical dimension at all and only their mechanical properties are of importance.
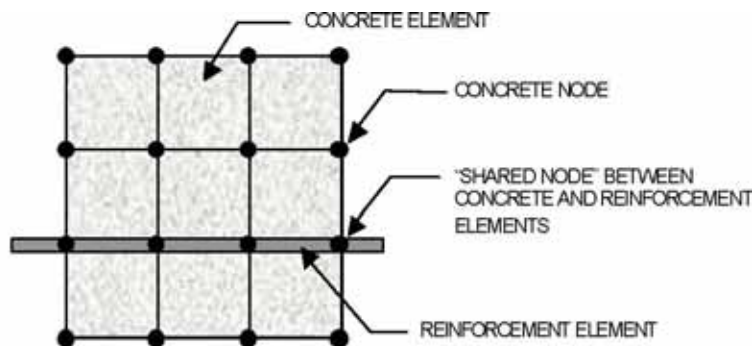

Figure 3: Shared nodes between concrete and reinforced elements

4.2   Embedded Model

To overcome mesh dependency in the discrete model, the embedded formulation allows independent choice of concrete mesh, as shown in Figure 4. In this approach, the stiffness of the reinforcing elements is evaluated independently from the concrete elements, but the element is built into the concrete mesh in such a way that its displacements are compatible with those of the surrounding concrete elements. That is, the concrete elements and their intersection points with each reinforcement segment are identified and used to establish the nodal locations of the reinforcement elements. In concrete structures, where reinforcement is complex, the embedded representation is advantageous. However, the additional nodes required for the reinforcement increase the number of degrees of freedom, and the hence the computational time. Although analyses with the embedded representation are in general more computationally efficient than those with the discrete representation, its application to the analysis of concrete structures is still expensive for day-to-day design.
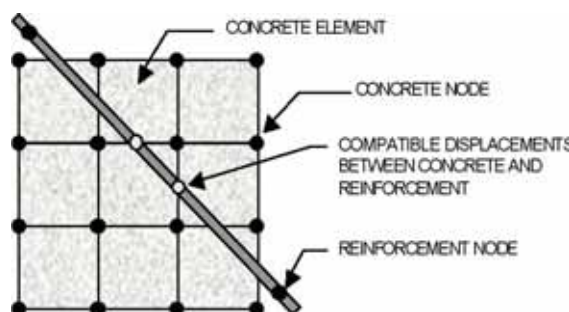
Figure 4: Embedded formulations for reinforced concrete

4.3   Smeared Model

In the smeared model, the reinforcement is assumed to be uniformly distributed over the concrete elements, as shown in Figure 5. As a result, the properties required by the material model in the element are constructed from individual properties of concrete and reinforcement by using composite theory. This technique is usually applied for large structural models, where reinforcement details are not essential to capture the overall response of the structure.
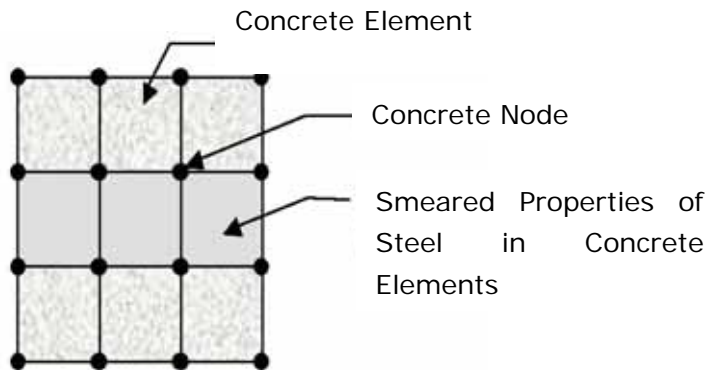
Figure 5: Smeared formulation for reinforced concrete

5   Nonlinear transient explicit finite element analysis

Explicit finite element method (FEM) was originally developed to solve problems in wave propagation and impact engineering, but they are currently used for many other applications such as sheet metal forming, underwater simulations, failure analysis, glass forming, metal cutting, pavement design, and earthquake engineering, among others [Chen$_{1982}$].

Implicit FEM is expensive, when thousands of time steps must be taken to solve a dynamic problem, because of the cost of inverting stiffness matrices to solve the large sets of nonlinear equations, especially for models with thousands of degrees of freedom or when nonlinearities are present. In an explicit FEM, the solution can be achieved without forming a global stiffness matrix. The solution is obtained on element-by-element basis and therefore global stiffness matrix need not be formed. As a result, explicit methods can treat large three-dimensional models (thousands of degrees of freedom) with comparatively modest computer storage requirements. Other advantages include easy implementation and accurate treatment of general nonlinearities. However, explicit methods are conditionally stable and therefore small time steps must be used. For stable computations, the time step is selected such that the time step is less than the time required for a stress wave to travel through the shortest element, and therefore this could result in excessive execution times as the level of discretization increases.

Central-difference method, which is characteristic of explicit methods in general, for direct time integration can be used. In this method, the solution is determined in terms of historical information consisting of displacements and time derivatives of displacements. By using this method, the finite element solution is then obtained

by using the following equations (with no damping):

$$\dot{u}^{n+1/2} = \dot{u}^{n-1/2} + \Delta t . M^{-1} \left(F^{external} - \int B^T \sigma dv \right) \tag{15}$$

$$u^{n+1} = u^{n-1} + \Delta t . \dot{u}^{n+1/2} \tag{16}$$

where $F^{external}$ is the vector of applied forces associated with the boundary conditions and body forces, M is the mass matrix, and $B^T \sigma dv$ is the internal force vector [Benson 2001]. In each time step the velocities and displacements are updated. In general, implicit methods have the form

$$u^{n+1} = f \left(\dot{u}^{n+1}, \ddot{u}^{n+1}, u^n, \cdots \right) \tag{17}$$

and therefore the computation of the current nodal displacements requires the knowledge of the time derivatives of u^{n+1}, which are unknown. Consequently, simultaneous equations need to be solved to compute the current displacements. On the other hand, explicit methods have the form

$$u^{n+1} = f \left(u^n, \dot{u}^n, \ddot{u}^n, u^{n-1}, \cdots \right) \tag{18}$$

and therefore the current nodal displacements can be determined in terms of completely historical information consisting of displacements and time derivatives of displacements at previous time steps. If a diagonal mass matrix is used, eqn. 18 is a system of linear algebraic equations and a solution is obtained without solving simultaneous equations. Once displacements are updated, strains can be computed, which are then used to determine stresses and eventually nodal forces. Stable integration by using the central difference method for undamped problems requires the following time step limit:

$$\Delta t \leq \frac{L}{C_w} \tag{19}$$

where L is related to the element size and c_w is the wave speed (speed at which stress waves travel in the element). The physical interpretation of this condition for linear displacement elements is that it must be small enough so that information does not propagate across more than one element in a time step. The shortcoming in using an explicit FEM, especially to model a quasi-static experiment is the fact that it can result in excessive execution times. Therefore, the time step will depend upon the shortest element size.

6   Numerical studies

Numerical studies have been carried out to compute the response of concrete target, due to impact of projectile. One example problem has been explained in detail.

Forrestal et al. (1994) conducted two sets of penetration experiments on concrete targets, which have compressive strengths of 23MPa and 39 MPa. The ogive nose projectiles were machined from 4340 Rc 45 steel and designed to contain a single channel acceleration data recorder. Impact analysis has been carried out taking these above mentioned dimensions and penetration depths for different velocities. In the discrete reinforcement model, reinforcement is modeled by using bar or beam elements connected to the concrete mesh nodes. As a result, there are "shared nodes" between the concrete and reinforcement mesh. Since the reinforcement is superimposed in the concrete mesh, concrete exists in the same regions occupied by the reinforcement. Parametric studies for penetration depth have also been carried out for various grades of concrete, CRHs and velocities. Design equations are proposed for computation of penetration depth after curve fit of the data by using MATLAB.

Details of the Projectile and Target

The geometry details of the projectile is shown in Figure 6.

Projectile characteristics

Material: Steel, Head: Ogive nose with caliber-radius-head = 3.0 and 6.0

Mass = 2.3kg

Geometry and FE modeling has been carried out by using general purpose FEA software, ANSYS. FE modeling has been carried out by employing Solid164 element, which has three DoF at each node, namely, u_x, u_y and u_z. Material model used is rigid material for the projectile. Distance between projectile and target is 5.92 inch (150.36 mm). Figure 7 shows the FE mesh of the target and projectile.

Target: The geometry of the target is made of concrete with compressive strength of concrete 23MPa, 40MPa and 60MPa. The target is in cylindrical shape. The height and diameters of cylinder are 71.48 in and 71.48 in respectively. Solid164 element has been employed to idealize target.

Total no. of elements in the mesh for target and projectile = 4887

Total no. of nodes in the mesh for target and projectile = 5865

The material model employed to represent the concrete is "Concrete Damage".

Table 1 shows input details of concrete damage model.

Contact algorithm employed between target and projectile is "surface-to-surface-automatic". Input details of projectile velocity are shown in Table 2. FEA has been
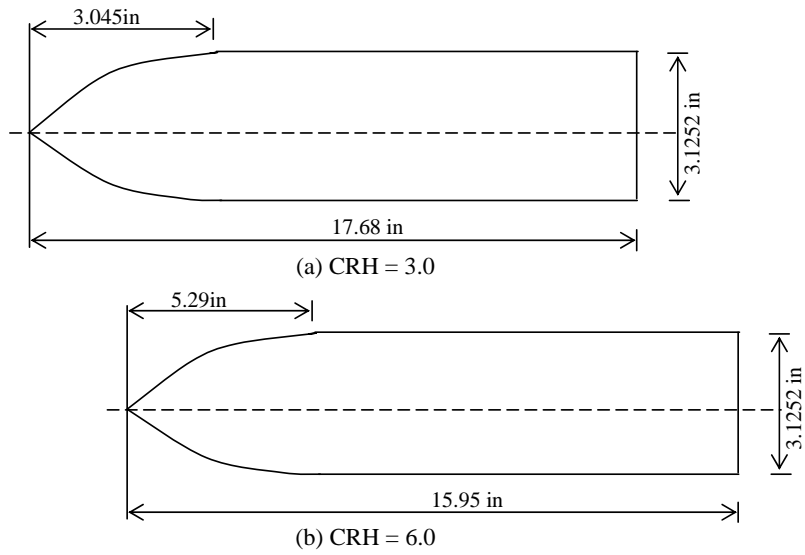
(a) CRH = 3.0

(b) CRH = 6.0

Figure 6: Projectile geometry details
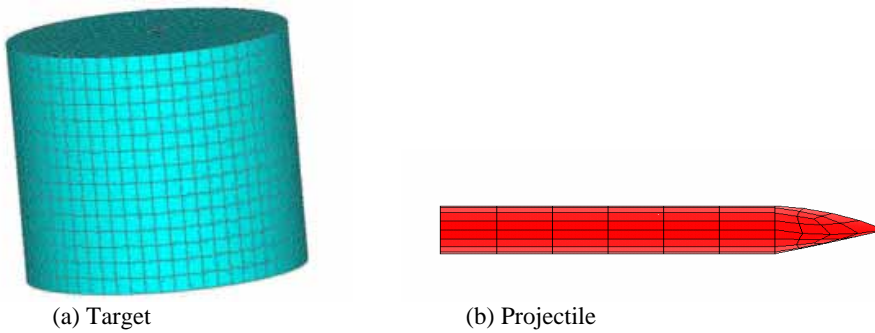

(a) Target   (b) Projectile

Figure 7: FE model of the Target and projectile

Table 1: Details of Concrete Damage material model

Mass density, RO	2.173e-4
Poisons ratio, PR	0.19
Max. principal stress for failure, SIGF	500 psi
Cohesion, AO	1478.0 psi
Pr. hardening coefficient, A1	0.4463
Pr. hardening coefficient, A2	0.1616e-4
Cohesion for yield, AOY	1116.0
Pr. hardening coefficient for yield limit, A1Y	0.625
Pr. hardening coefficient for yield material, A2Y	0.515e-4
Pr. hardening coefficient for failed material, A1F	0.4417
Pr. hardening coefficient for failed material, A2F	0.2366e-4
Damage scale factor, B1	15.0
Damage scale factor for uniaxial tensile path, B2	50.0
Damage scale factor for triaxial tensile path, B3	0.01

Damage function coefficients

$X_1 – 0$	$X_7 – 0.8e-4$	$X_{13} – 0.1e+11$
$X_2 – 0.8e-5$	$X_8 – 0.32e-3$	
$X_3 – 0.24e-4$	$X_9 – 0.52e-3$	
$X_4 – 0.4e-4$	$X_{10} – 0.57e-3$	
$X_5 – 0.56e-4$	$X_{11} – 0.1e+1$	
$X_6 – 0.72e-4$	$X_{12} – 0.1e+2$	

Scale factor values

$X_1 – 0$	$X_7 – 0.97$	$X_{13} – 0$
$X_2 – 0.85$	$X_8 – 0.5$	
$X_3 – 0.97$	$X_9 – 0.1$	
$X_4 – 0.99$	$X_{10} – 0$	
$X_5 – 1.0$	$X_{11} – 0$	
$X_6 – 0.99$	$X_{12} – 0$	

$E_0 = 0$, Gamma = 0: $V_0 = 1.0$

Volumetric strain data values		Volumetric pressure values	
$\varepsilon_{v1} – 0$	$\varepsilon_{v6} – -3.2e-2$	$C_1 – 0$	$C_6 –0.1017e+5$
$\varepsilon_{v2} – -0.6e-2$	$\varepsilon_{v7} – -0.788e-1$	$C_2 – 0.325e+4$	$C_7 – 0.1667e+5$
$\varepsilon_{v3} – -1.08e-2$	$\varepsilon_{v8} – -3.56e-1$	$C_3 – 0.4973e+4$	$C_8 – 0.7053e+5$
$\varepsilon_{v4} – -1.72e-2$	$\varepsilon_{v9} – 0.4e+1$	$C_4 – 0.7086e+4$	$C_9 – 0.7213e+6$
$\varepsilon_{v5} – -2.4e-2$	$\varepsilon_{v10} – -0.4e+4$	$C_5 – 0.8906e+4$	$C_{10} – 0.7213e+6$

carried out by using NONSTRANS module of FINEART software and the results are viewed in LS-PREPOST. The predicted penetration depth values for different velocities are in good agreement with the corresponding experimental values available in the literature.

Target Concrete Model with Reinforcement

0.6% of reinforcement is taken into account for the same concrete target model.

Figure 8 shows the FE model of concrete with smeared and discrete model for reinforcement.

(a) Smeared reinforcement model (b) Discrete reinforcement model

(a) Smeared reinforcement model   (b) Discrete reinforcement model
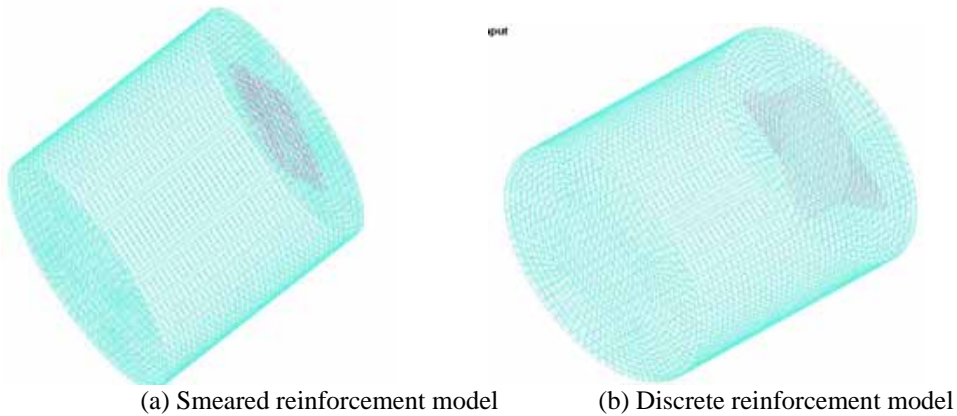
Figure 8: FE model of concrete target

Parametric studies

Parametric studies have been conducted to compute penetration depth. The parameters include impact velocities, grades of concrete and CRHs. Penetration depth is computed by employing all the three schemes, namely, option model, smeared model and discrete model. Penetration depth is also computed for the case of without reinforcement. The percentage of reinforcement adopted for the study is 0.6. The computed penetration depths for various velocities are given in Table 2 for CRH =3 and 6.

From the above parametric studies, it can be observed that

- Penetration depth decreases with the increase of grade of concrete

- Penetration depth increases with the increase of CRH

- Penetration depth increases with increase of velocity

- The difference between the computed penetration depth with and without accounting the effect of reinforcement for 0.6% is approximately 10%

- The computed penetration depth by using discrete model falls in between the option model and smeared model.

Figures. 9(a) to (x) show the velocity vs. penetration depth for 23MPa, 40MPa and 60MPa with and without reinforcement. These plots are obtained by curve fitting the data by using MATALB software.

Table 2a: Comparison of penetration depth (mm) (CRH=3)

Velocity (m/s)	Without reinforcement	0.6% reinforcement		
		Option model	Smeared model	Discrete model
23 MPa, 3CRH				
139	228(240)	187	160	171
200	390 (420)	343	320	329
250	550	508	471	483
300	832	782	745	749
336	877(930)			
350	960	915.25	892	901
378.6	1080(1180)			
300	1285	1189	1144	1170
40 MPa, 3CRH				
139	180	160	145	153.5
200	230	206	175	184
250	350	316	273	285
275.7	365(380)			
300	412	365	341	351
350	415	423	383	408
400	663	616	570	594
456.4	865(940)			
450	825	747	705	725
550	1416	1345	1293	1301
60 MPa, 3CRH				
139	135	110	88	105
200	160	137	112	127
250	251	220	176	197
300	343	307	264	294
350	447	397	351	373
400	512	469	436	460
450	731	682	657	668
550	1280	1230	1187	1209

- ()- The values given in bracket correspond experimental observations [Forrestal et al. 1994].
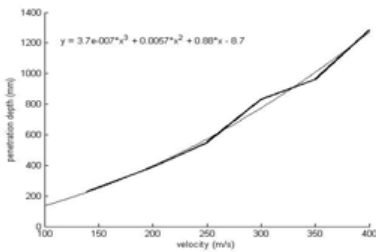
(a) 23MPa, 3CRH no reinforcement
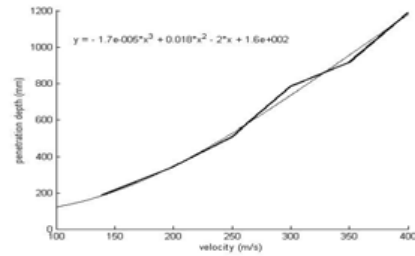
(b) 23MPa, 3CRH, 0.6 %of reinforcement option model
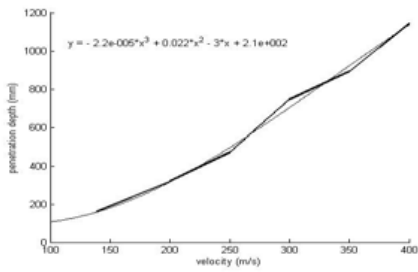
(c) 23MPa, 3CRH 0.6% reinf. smeared model
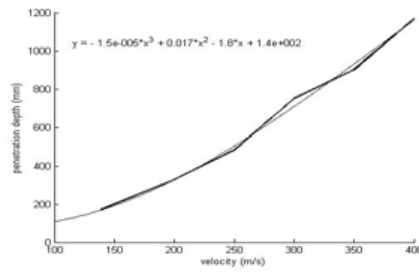
(d) 23MPa, 3CRH 6% reinf. discrete model
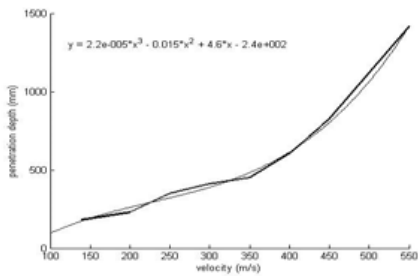
(e) 40MPa, 3CRH no reinf.
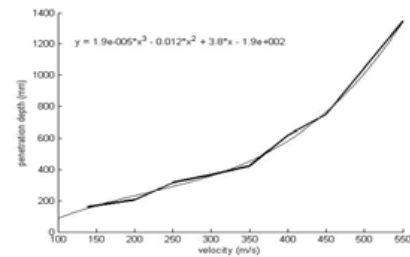
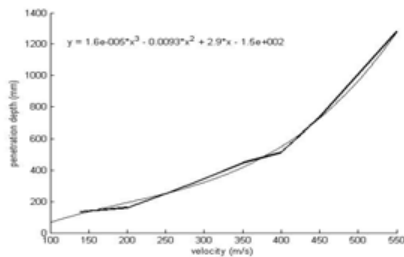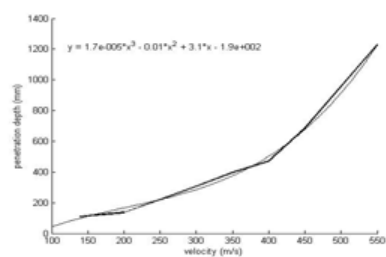

(f) 40MPa, 3CRH 0.6% reinf. option model
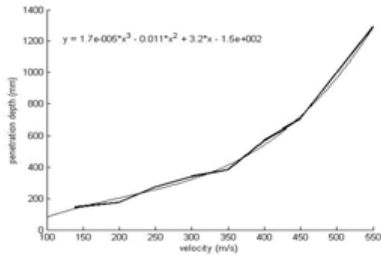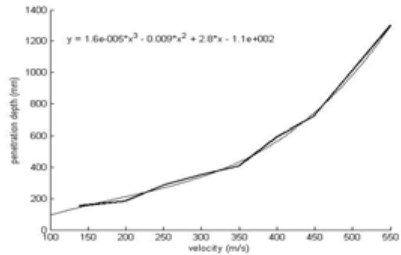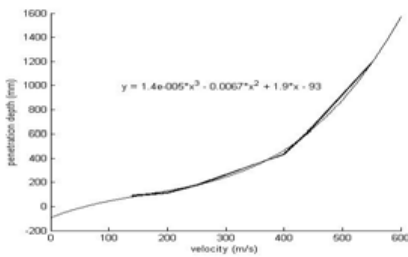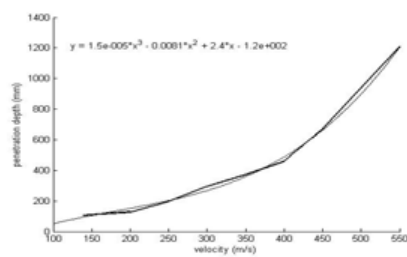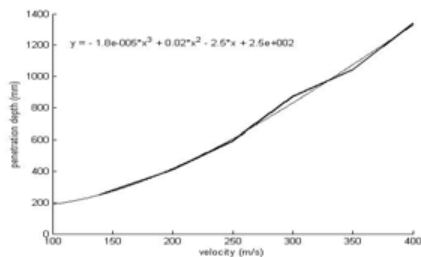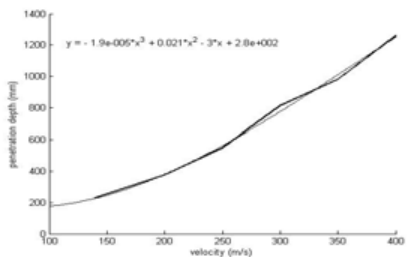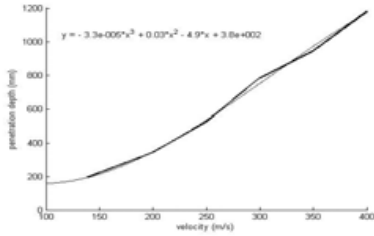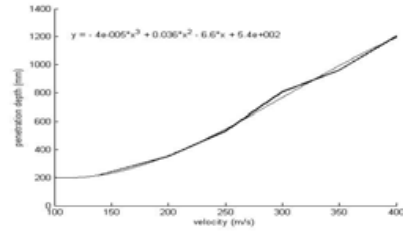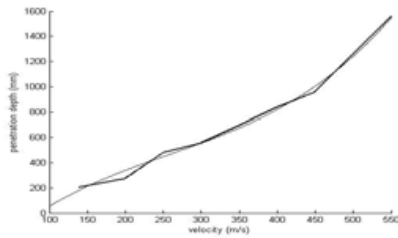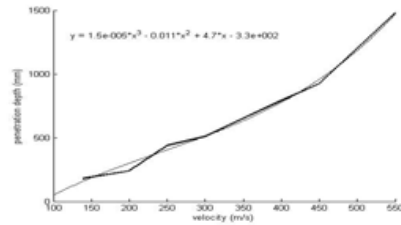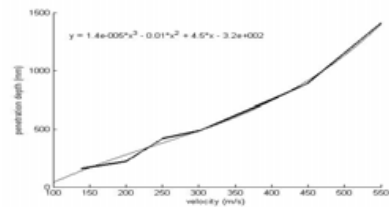
(g) 40MPa, 3CRH 0.6% reinf. smeared model   (h) 40MPa, 3CRH 0.6%reinf. discrete model

(i) 60MPa, 3CRH no reinf.   (j) 60MPa, 3CRH 0.6% reinf. option model

(k) 60MPa, 3CRH 0.6% reinf. smeared model   (l) 60MPa, 3CRH 0.6%reinf. discrete model

(m) 23MPa, 6CRH no reinf.   (n) 23MPa, 6CRH 0.6% reinf. Option model

(o) 23MPa, 6CRH 0.6% reinf. smeared model   (p) 23MPa, 6CRH, 0.6% reinf. Discrete model
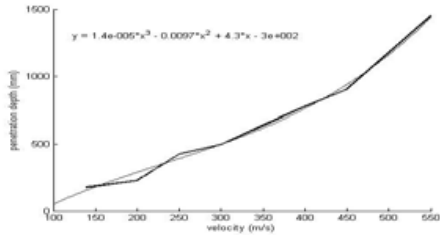
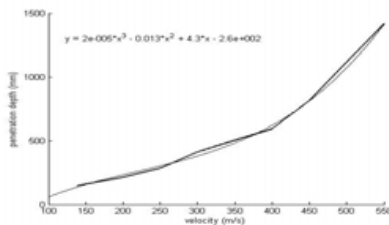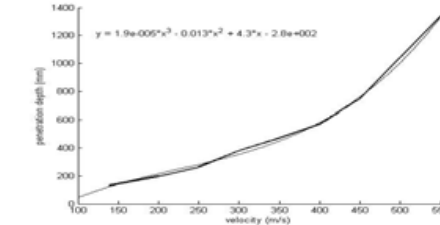(q) 40MPa, 6CRH no reinf   (r) 40MPa, 6CRH 0.6% reinf. option model

(s) 40MPa, 6CRH 0.6% reinf. smeared model   (t)40MPa, 6CRH 0.6% reinf. discrete model
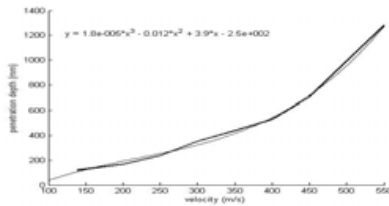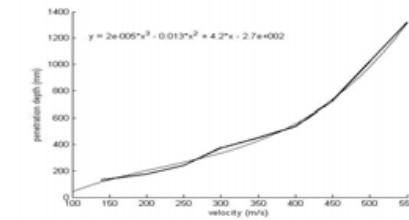
(u) 60MPa, 6CRH no reinf.   (v) 60MPa, 6CRH 0.6% reinf. option model

(w) 60MPa, 6CRH 0.6% reinf. smeared model   (x) 60MPa, 6CRH, 0.6% reinf. discrete model

Figure 9: Variation of penetration depth w.r.to impact velocity

Table 2b: Comparison of penetration depth (mm) (CRH=6)

Velocity (m/s)	Without reinforcement	0.6% reinforcement		
		Option model	Smeared model	Discrete model
23 MPa, 6CRH				
139	251	228	197	219
200	411	376	343	352
238.4	569(580)			
250	594	548	525	530
300	870	813	783	806
350	1043	981	945	960
378	1130(1250)			
400	1335.89	1259	1180	1203
39 MPa, 6CRH				
139	205	180	160	176
200	275	241	220	228
250	480	440	417	425
300	558	510	483	496
312.5	603(610)			
350	695	652	615	637
400	838	791	747	775
450	960 (990)	923	890	902
550	1560	1480	1410	1450
60 MPa, 6CRH				
139	147	132	120	130
200	215	197	167	175
250	283	263	237	241
300	411	380	351	374
350	503	470	439	450
400	594	570	527	536
450	812	747	703	723
550	1418	1340	1280	1320

- * The values given in bracket correspond to experimental observations [Forrestal et al.1994].

The following expressions have been obtained after regression analysis of impact velocity vs penetration depth data by using MATLAB software

1. 23MPa, 3CRH and no reinforcement

$$Y = 3.7e - 007 * x^3 + 0.0057 * x^2 + 0.88 * x - 8.7 \tag{20a}$$

2. 23MPa, 3CRH 0.6% reinforcement and option model

$$Y = -1.7e - 005 * x^3 + 0.018 * x^2 - 2 * x + 1.6e + 2 \tag{20b}$$

3. 23MPa, 3CRH 0.6% reinforcement and smeared model

$$Y = -2.2e - 005 * x^3 + 0.022 * x^2 - 3 * x + 2.1e + 2 \tag{20c}$$

4. 23MPa, 3CRH 0.6% reinforcement and discrete model

$$Y = -1.5e - 005 * x^3 + 0.017 * x^2 - 1.8 * x + 1.4e + 2 \tag{20d}$$

5. 40MPa, 3CRH and no reinforcement

$$Y = 2.2e - 005 * x^3 - 0.015 * x^2 + 4.6 * x - 2.4e + 2 \tag{20e}$$

6.40MPa, 3CRH 0.6% reinforcement and option model

$$Y = 1.9e - 005 * x^3 - 0.012 * x^2 + 3.8 * x - 1.9e + 2 \tag{20f}$$

7. 40MPa, 3CRH 0.6% reinforcement and smeared model

$$Y = 1.7e - 005 * x^3 - 0.011 * x^2 + 3.2 * x - 1.5e + 2 \tag{20g}$$

8. 40MPa, 3CRH 0.6%reinforcement and discrete model

$$Y = 1.6e - 005 * x^3 - 0.009 * x^2 + 2.8 * x - 1.1e + 2 \tag{20h}$$

9. 60MPa, 3CRH and no reinforcement

$$Y = 1.6e - 005 * x^3 - 0.0093 * x^2 + 2.9 * x - 1.5e + 2 \tag{20i}$$

10. 60MPa, 3CRH 0.6%reinforcement and option model

$$Y = 1.7e - 005 * x^3 - 0.01 * x^2 + 3.1 * x - 1.9e + 2 \tag{20j}$$

11. 60MPa, 3CRH 0.6%reinforcement and smeared model

$$Y = 1.4e - 005 * x^3 - 0.0067 * x^2 + 1.9 * x - 93 \tag{20k}$$

12. 60MPa, 3CRH 0.6%reinforcement and discrete model

$$Y = 1.7e - 005 * x^3 - 0.01 * x^2 + 3.1 * x - 1.9e + 2 \tag{20l}$$

13. 23MPa, 6CRH and no reinforcement

$$Y = 1.5e - 005 * x^3 - 0.0081 * x^2 + 2.4 * x - 1.2e + 2 \tag{20m}$$

14. 23MPa, 6CRH 0.6%reinforcement and opt model

$$Y = 1.8e - 005 * x^3 - 0.02 * x^2 - 2.5 * x + 2.5e + 2 \tag{20n}$$

15. 23MPa, 6CRH 0.6%reinforcement and smeared model

$$Y = 1.9e - 005 * x^3 - 0.021 * x^2 + 3 * x + 2.8e + 2 \tag{20o}$$

16. 23MPa, 6CRH 0.6%reinforcement and discrete model

$$Y = -3.3e - 005 * x^3 - 0.03 * x^2 - 4.9 * x + 3.8e + 2 \tag{20p}$$

17. 40MPa, 6CRH and no reinforcement

$$Y = -4e - 005 * x^3 + 0.036 * x^2 - 6.6 * x + 5.4e + 2 \tag{20q}$$

18.40 MPa, 6CRH 0.6%reinforcement and opt model

$$Y = 15e - 005 * x^3 - 0.011 * x^2 + 4.7 * x - 3.3e + 2 \tag{20r}$$

19. 40MPa, 6CRH 0.6%reinforcement and smeared model

$$Y = 1.4e - 005 * x^3 - 0.01 * x^2 + 4.5 * x - 3.2e + 2 \tag{20s}$$

20. 40MPa, 6CRH 0.6%reinforcement and discrete model

$$Y = 1.4e - 005 * x^3 - 0.0097 * x^2 + 4.3 * x - 3e + 2 \tag{20t}$$

21. 60MPa, 6CRH and no reinforcement

$$Y = 2e - 005 * x^3 - 0.013 * x^2 + 4.3 * x - 2.6e + 2 \tag{20u}$$

22. 60 MPa, 6CRH 0.6%reinforcement and opt model

$$Y = 1.9e - 005 * x^3 - 0.013 * x^2 + 4.3 * x - 2.8e + 2 \tag{20v}$$

23. 60 MPa, 6CRH 0.6%reinforcement and smeared

$$Y = 1.8e - 005 * x^3 - 0.012 * x^2 + 3.9 * x - 2.5e + 2 \tag{20w}$$

24. 60MPa, 6CRH 0.6%reinforcement and discrete model

$$Y = 2e - 005 * x^3 - 0.013 * x^2 + 4.2 * x - 2.7e + 2 \tag{20x}$$

where Y = penetration depth, mm, x = impact velocity, m/s

Figure 10 shows the penetration of projectile into concrete target and contour of σ_{zz} stress for concrete target without and with reinforcement model by using different schemes for projectile impact velocity of 139 m/s.
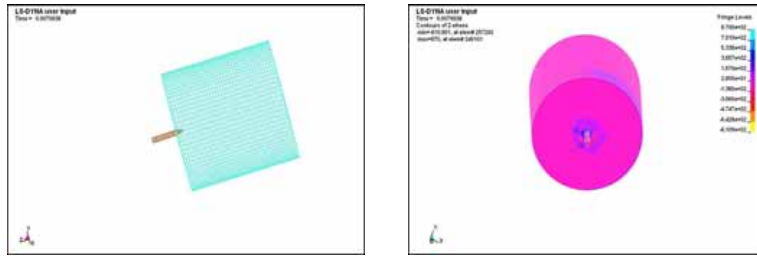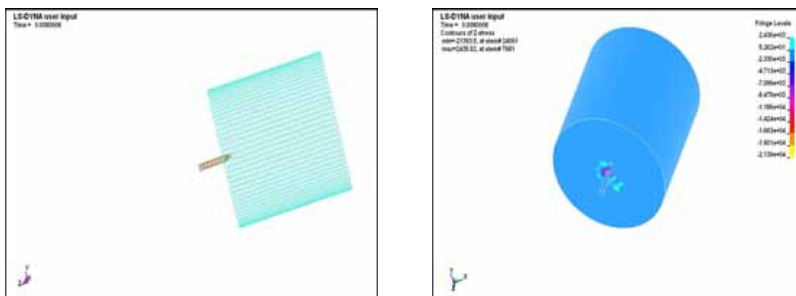
(a) Plain Concrete Target without reinforcement
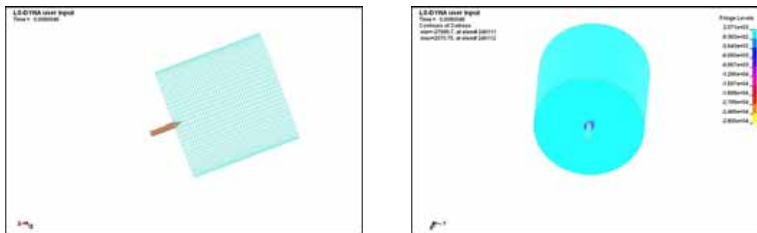
(b) Concrete Target with Reinforcement – option model
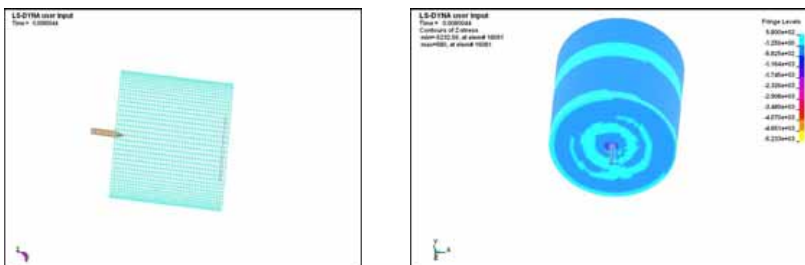
(c) Concrete Target with Reinforcement – smeared model

(d) Concrete Target with Reinforcement – discrete model

Figure 10: Penetration of projectile into concrete and σ_{zz} stress contour

7   Summary & concluding remarks

Nonlinear transient dynamic projectile impact analysis has been carried out for concrete structural components. Concrete damage model has been employed to simulate the nonlinear behaviour of concrete. Various contact algorithms used to model the interface between the projectile and target have been discussed. Brief note on equation-of-state is provided. Various modelling schemes of reinforcement are explained. The procedure for nonlinear transient explicit FEA has been presented. Based on the methodologies, program modules have been developed and integrated with the NONTRANS module of FINEART.

Parametric studies have also been carried out on various grades of concrete, CRHs and velocities. Based on the studies, the following observations are made:

- Penetration depth decreases with the increase of grade of concrete

- Penetration depth increases with the increase of CRH

- Penetration depth by using discrete model falls in between the option model and smeared model.

The data obtained from the parametric studies (i.e velocity vs penetration depth) has been used for curve fitting in MATLAB. After regression analysis, design expressions are proposed for computation of penetration depth. These expressions will be useful for designers to compute the penetration depth under projectile impact loading.

References

AUTODYN v4.2 (2001): User manual, Century Dynamics, Inc.

Benson, D. (2001): A Brief Introduction to Explicit Finite Element Methods. FEA Informational News, vol. 2-3.

Chen W.F. (1982): Plasticity in Reinforced Concrete. McGraw Hill, Inc., New York.

Farnam, Y.; Soheil Mohammadi, Mohammad Shekarchi. (2010): Experimental and numerical investigations of low velocity impact behavior of high-performance

fiber-reinforced cement based composite, *Int J Impact Eng*, vol. 37, no.2, pp. 220-229.

Forrestal, M.J.; Altman, B.S.; Cargile, J.D.; Hanchak, S.J. (1994): An empirical equation for penetration depth of ogive-nose projectiles into concrete targets. *Int Jl Impact Engg*, vol. 15, no.4, pp. 395–405.

Govindjee, S.; Kay, G.J.; Simo, J.C. (1994): Anisotropic modeling and numerical simulation of brittle damage in concrete. Report Number UCB/SEM M-94/18. Berkeley, CA: University of California at Berkeley, Department of Civil Engineering.

Govindjee, S.; Kay, G.J.; Simo, J.C. (1995): Anisotropic modeling and numerical simulation of brittle damage in concrete. *Int. J Numer Meth Engg*, vol. 38, pp. 611–33.

Hentz, S.; Donze, F.V.; Daudeville, L. (2004): Discrete element modeling of concrete submitted to dynamic loading at high strain rates. *Comput Struct*, vol.82, no.29–30, pp. 2509–24.

LS-DYNA (2003): Keyword user's manual, version 970, Livermore Software Technology Corporation.

Malvar, L.J.; Crawford, J.E.; Wesevich. (1997): A plasticity concrete material model for Dyna3D. *Int J Impact Eng*, vol. 19, no.9–10, pp. 847–73.

Malvar, L.J.; Crawford, J.E.; Wesevich, J.W.; Simons, D.A. (1994): New concrete material model for DYNA3D. TM-94-14.3 Report to the Defense Nuclear Agency Glendale, C. A: Karagozian and Case Structural Engineers.

Malvar, L.J.; Crawford, J.E.; Wesevich, J.W.; Simons, D.M. (1996): A new concrete material model for DYNA3D release II: shear dilation and directional rate enhancements. TM-96-2.1, Report to the Defense Nuclear Agency. Glendale, CA: Karagozian and Case Structural Engineers.

Rama Chandra Murthy, A.; Palani, G.S.; Nagesh R. Iyer, Rajasankar, J.; Smitha Gopinath, Cinitha, A. (2008): State-of-the Art review on Concrete Structural Components Subjected to Impact Loading, SERC Research Report No. CSD-MLP134-RR-01.

Rama Chandra Murthy, A.; Palani, G.S.; Nagesh R. Iyer, Rajasankar, J.; Smitha Gopinath. (2009): Impact analysis of concrete structural components using empirical and analytical approaches. SERC Research Report No. CSD-MLP134-RR-03.

Tu, Z.; Lu, Y. (2009): Evaluation of typical concrete material models used in hydrocodes for high dynamic response simulations. *Int Jl Impact Engg*, vol. 36, pp. 132-146.

Yonten, K.; Majid, T.M.; Marzougui, D.; Eskandarian, A. (2005): An assessment of constitutive models of concrete in the crashworthiness simulation of roadside safety structures, *Int J Crashworthiness*, vol. 10, no. 1, pp. 5–19.